Hygiene and Environmental Health Advances 8 (2023) 100083

Contents lists available at ScienceDirect

Hygiene and Environmental Health Advances

journal homepage: www.elsevier.com/locate/heha

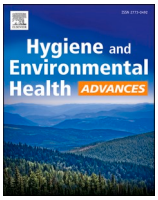

Possible hazardous components in dental alginates: Physicochemical properties by a mineralogical and spectroscopic investigation

Matteo Ardit [a], Tommaso Baroni [b,*], Fabio Capacci [c], Giulio Arcangeli [d], Maurizio Romanelli [b], Alfonso Zoleo [e], Silvana Capella [f], Elena Belluso [f], Pietro Gabellini [b], Raffaello Cioni [b], Francesco Di Benedetto [a]

[a] Department of Physics and Earth Sciences, University of Ferrara, Ferrara, Italy
[b] Department of Earth Sciences, University of Florence, Florence, Italy
[c] Health Agency of Florence, Florence, Italy
[d] Department of Clinical and Experimental Medicine, University of Florence, Florence, Italy
[e] Department of Chemical Sciences, University of Padova, Padova, Italy
[f] Department of Earth Sciences and Scansetti Research Centre, University of Turin, Turin, Italy

ARTICLE INFO

Keywords:
Alginate impression materials
Cristobalite
Wollastonite
Respirable fraction
Spectroscopy

ABSTRACT

Alginates are products used as impression materials in dentistry and prosthetics. They consist of polymers, calcium alginates mixed with diatomite and additives. Recently, the occurrence of severe silicosis associated with exposure to respirable dust of such materials has increased the scientific interest in understanding how these materials may pose a toxicological problem to workers. The primary objective of this study is to improve the understanding of both the existence and the characteristics of the toxicant(s) contained in these materials, with the goal of better defining the risk assessment for this occupational setting.

Two commercial dental alginates were subjected to a mineralogical, microchemical and spectroscopic investigation. The results indicate the presence of a significant amount of diatomite, clearly identified by micromorphology and formed mainly by cristobalite. The respirable fraction of the dust represents at least 30 % of the total number of particles, and this fraction contains a relevant amount of crystalline silica particles. Conversely, the investigated alginate materials do not exhibit the presence of radical species.

The results obtained confirm that the cristobalite detected originates from the high-temperature transformation of amorphous silica during the calcination process of diatomite, prior to mixing with the other components. The same process also produces wollastonite ($CaSiO_3$), which, like cristobalite, is a crystalline phase known for its toxicological effects. The present findings call for a rethinking of dental alginates with regard to the definition of their health risks for technical operators.

Introduction

Calcium alginates are impression materials composed of elastic, irreversible hydrocolloids that have numerous applications in medicine, especially in dentistry (Cook, 1986; Porrelli et al., 2020), and in prosthesis manufacturing (Hattab, 2019; Yamamoto et al., 2019; Czechowska et al., 2020). In addition, their specific technological properties combined with their non-toxicity make alginates effective in industrial pharmaceutical applications as drug delivery systems (Hattab, 2019, and references therein).

Alginate is a soluble salt of alginic acid, a colloidal polysaccharide extracted from marine kelp (brown seaweed plant). Alginates can undergo a gelation reaction when the polymer filaments are bridged by Ca^{2+} ions in solution (Cook, 1986). Commercial alginates are based on a mixture of dried materials, namely polysaccharides of two main monosaccharides (*i.e.*, d-mannuronate and l-guluronate), to which calcium sulfate dihydrate, $CaSO_4{\cdot}2H_2O$ (gypsum, Cook, 1986; Czeschowska et al., 2020) is added. The latter phase is added as a heterogeneous source of Ca^{2+} released during the mineral dissolution in water. The final formulation of commercial alginates also includes some additives, such as:

* Corresponding author.
E-mail address: tommaso.baroni@unifi.it (T. Baroni).

https://doi.org/10.1016/j.heha.2023.100083

Available online 13 November 2023

- ✓ a pH modifier (usually MgO, periclase),
- ✓ a reaction retarder ($Na_4P_2O_7$, which can compete with the alginate for the complexation of Ca^{2+} ions),
- ✓ a reaction modifier (Na_2TiF_6, which can accelerate the dissolution of Ca sulfate and provide a more compact and dense impression profile).

The mechanical strength of the reaction mixture is provided by diatomite (or diatomaceous earth), another natural inert additive used as a filler and consisting primarily of amorphous SiO_2 (Cook, 1986). Diatomite has been the subject of a long series of epidemiological studies (*e.g.*, Checkoway et al., 1993; Picciotto et al., 2018) because it is largely converted to cristobalite (crystalline SiO_2) after calcinations at temperatures above 800 °C to improve its mechanical properties.

Respirable particles of cristobalite, such as respirable α-quartz dust (the most common silica polymorph), are toxic to humans. They cause pneumoconiosis (silicosis) and autoimmune diseases and are classified as human carcinogens (IARC, 2012). To date, diatomite production is the only occupational setting in which cohorts of workers with silicosis have been epidemiologically linked to exposure to cristobalite as the dominant respirable dust (Checkoway et al., 1993). Nevertheless, recent studies of severe pneumoconiosis diagnosed in cohorts of artificial stone production workers have provided evidence of a non-negligible fraction of cristobalite in the processed materials (Di Benedetto et al., 2019, 2020).

A recent study by Barbieri et al. (2020) first reported the case of a deceased worker with severe silicosis whose exposure was associated with the production of dental alginates. These authors suggested that this work environment is critical for crystalline silica exposure, particularly for respirable cristobalite dust. To the authors' knowledge, there are no other reports in the literature. Accordingly, the present study was designed to improve the understanding of both the presence and the characteristics of the toxicant(s) contained in alginate materials, in order to better define the risk assessment for this occupational setting. This objective was pursued by studying two commercial calcium alginate mixtures through in-depth mineralogical, chemical and spectroscopic analyses (including X-ray powder diffraction, XRPD; scanning electron microscopy, SEM, micromorphology coupled to energy dispersive system, EDS, microanalysis; micromorphometric characterization by image analysis; electron paramagnetic resonance, EPR, spectroscopy; and transmission electron microscopy, TEM, microstructural investigations) to quantify the amount of cristobalite and the amount of respirable fraction of the dust.

Materials and methods

Materials

Two commercial samples of dental alginates (hereafter referred to as A1 and A2) were provided by the Occupational Surveillance Service (OSS) of the Health Agency of Florence (Italy). Samples consist of very fine (impalpable) dry powders. Constituents of the samples, as reported in the corresponding datasheets, are listed in Table 1. Powders were kept in a dry box, to avoid any reaction due to humidity (in particular, to avoid the dissolution of the gypsum and the subsequent hardening of the alginate).

Table 1
Constituents of the investigated samples as declared in the supplied OSS datasheets. N.d. – not declared.

Phase	sample A1 *Wt % range*	sample A2 *Wt % range*
Kieselguhr (diatomite)	50–75	65–80
K fluortitanate, K_2TiF_6	0–5	1.0–2.5
cristobalite	–	1–10
Talc	*n.d.*	–
Periclase	*n.d.*	–

X-Ray powder diffraction (quantitative phase analysis, QPA-XRPD)

Prior to XRPD measurements, each sample was mixed with 15 wt % corundum (NIST alumina powder SRM 676) as an internal standard for the quantification of the crystalline phases and XRD amorphous content, and ground in an agate mortar and pestle (Snyder and Bish, 1989; Gualtieri et al., 2014). Data collection was performed at room temperature on a Bruker D8 Advance Da Vinci diffractometer operating in Bragg-Brentano geometry and equipped with a Cu-anode X-ray tube, Ni-filter to suppress the Cu$K\beta$ component, and a LynxEye XE silicon strip detector (2.585° of window size) set to discriminate the Cu$K\alpha_{1,2}$ radiation (available at the Physics and Earth Sciences Department of University of Ferrara). The powder of each sample was scanned in a continuous mode in the 5–90° 2θ angular range with a step size of 0.02° 2θ and a counting time of 3 s per step. A knife perpendicular to the sample was placed at a suitable distance from the sample surface to reduce the air-induced scattering.

Qualitative phase analysis was performed using EVA v.6 software (Bruker). Collected XRPD patterns were modeled using the fundamental-parameter Rietveld approach (TOPAS v.5, Bruker). Since the certified weight percentage of crystalline corundum SRM 676 is 91.75(±1.52) wt %, the weight fraction of crystalline corundum used as an internal standard to obtain the correct value of the amorphous fraction of the investigated samples was kept constant at 13.76 wt % during the refining procedure (*i.e.*, corundum was treated as a spiked phase with a crystalline phase fraction of 15 wt % * 0.9175 = 13.76 wt %). All the identified phases were modeled by performing multiphase refinements. Known instrumental parameters (*e.g.*, goniometer radius, slit sizes, X-ray tube geometric parameters, etc.) were used to calculate the instrumental contribution to the peak profiles, the zero-error correction was fixed at the value determined using the NIST Si standard (SRM 640e), and refinements included a sample displacement correction and a Chebyshev polynomial curve to model the background.

Scanning electron microscopy

Sample aliquots were placed on aluminum stubs using double-sided conductive adhesive tape and coated with graphite. Secondary electron micrographs were obtained using a ZEISS EVO MA15 SEM (available at the MEMA center, Centro di Microscopia e Microanalisi, at the University of Florence) with an accelerating voltage of 20 kV. Energy dispersive spectrometry (EDS) microanalysis was performed using an INCA 250 Oxford spectrometer coupled to the microscope. Peaks were fitted by Gaussian curves using the ZAF (atomic number, absorption, fluorescence) correction. Calibration was performed with respect to a Co reference sample.

Grain size and particle morphology

Grain size distribution of both samples was obtained through image analysis using an automatic static particle analyzer (Malvern Morphologi 3Gs) at the VuLab (Volcanology laboratory) of the Earth Science Department of University of Florence. A small aliquot (7 to 11 mm^3) of each powder was dispersed by an impulsive jet of compressed air over a glass slide, and the particles were then automatically recognized and measured by the instrument. For each sample, a set of fundamental morphometric parameters was measured using the apparent projected shape of a large number of grains (in the order of 10^5). The size of each grain was quantified as the diameter of the equivalent circle (particle diameter) of the projected shape. To maximize data accuracy and to minimize operator error, the analyses were performed using a standard operating procedure (SOP) calibrated with a high-resolution optic (20X magnification). A total of 4 replicate analyses were performed on each sample to account for the natural variability of the samples.

The grain size distribution (GSD) of the two samples was calculated considering both the cumulative fraction of the particle volume (NVF: normalized volume frequency) and the particle number (NNF: normalized number frequency). The GSD was averaged considering the repeated analyses, and the associated uncertainty was estimated as the maximum and minimum value of NVF and NNF measured for each particle diameter.

The "thoracic" inhalable (< 10 μm) and respirable (< 4 μm) fractions (Brown et al., 2013) of the investigated samples were quantified as the values of NVF and NNF for the GSD curves and reported with the associated uncertainties. Using the particle analyzer, a set of dimensionless shape parameters (Leibrandt and Le Pennec, 2015) was also automatically measured for each grain in order to provide the shape analysis of the particles as a function of their grain size. Two parameters were chosen to better reflect the morphological variability of the particles: Elongation $Elng = 1 - W_P/L_P$, where W_P and L_P are the particle width and length, respectively, and Solidity $SLD = A_{CH}/A_P$ where A_{CH} and A_P are the area of the Convex Hull (the minimum convex envelope containing the particle) and the area of the particle, respectively (Leibrandt and Le Pennec, 2015). While *Elng* is an unambiguous measure of particle shape, *SLD* is a parameter which describes the presence of important embayments of the external contour of a particle. Due to the very large number of particles measured by the instrument, to represent the shape variability of the particles with size we calculated the simple moving average (SMA) of the different parameters over a moving window of 200 particles, after ordering by size the particles. SMA plots for *Elng* and *SLD* are then presented.

Electron paramagnetic resonance

Samples were analyzed without pretreatment or manipulation. An aliquot of the dry powder was placed in amorphous silica tubes using Teflon bags. The tubes were chosen to avoid the presence of transition metal impurities (mainly Fe or Cr) in the glassy matrix, which are likely to interfere with the EPR spectra of the samples. EPR spectral measurements were performed at both room and low temperature. Room temperature EPR spectra were collected with a conventional Bruker ER 200D-SRC, operating at ~9.5 GHz (X-band), available at the Department of Chemistry of the University of Florence. Spectra were recorded at 0.4 mT modulation amplitude, 100 KHz modulation frequency. The post-amplification gain setup was optimized to maximize the signal-to-noise ratio. All spectra were recorded in a magnetic field range of 0–1000 mT, with a field step of 4.885 mT, and at a scan speed of 0.098 mT/s.

Low temperature EPR spectra were collected at the Department of Chemical Sciences of the University of Padua using a Bruker ELEXYS X-band EPR equipped with an Oxford CF935 cryostat and a dielectric cavity with high Quality (Q) factor. The measurements were performed at 80 K. Spectra were recorded in the magnetic field range 50–650 mT (panoramic spectra) and 320–360 mT (detailed spectra), with a modulation amplitude of 0.05 mT and a modulation frequency of 100 kHz.

Transmission electron microscopy

Transmission electron microscopy (TEM) was used to investigate the size, morphology, crystallinity, and chemical composition of the particles using a Philips CM12 instrument operating at 120 kV with a LaB_6 filament coupled to an EDS microanalysis probe (Genesis 2000 system with TEM Quant software PV8206/31 processing system, available at the Department of Earth Sciences, University of Turin).

For experimental purposes, a small amount of each powder was mixed with pure acetone, and sonicated for 10 min; two drops of the resulting suspension were deposited on a copper mesh grid coated with a 200 Å carbon film. The first attempt to obtain a suspension by mixing the powder with isopropyl alcohol failed, probably due to the presence of water in the alcohol; in fact, the sample appeared as a continuous patina in the TEM.

About 20 grains were examined for each sample. For each grain, TEM images from low to high magnification were observed to measure size and define morphology, and electron diffraction was processed to evaluate the crystallinity or the amorphous state.

Results

Grain size and morphology

Grain size distribution (GSD) of the investigated samples is shown in Fig. 1 (a-b) and (c-d) as %number and %volume of particles, respectively. The two alginate powders show a similar grain size distribution, with 6–10 vol % of the total deposit (corresponding to an average of 70–85 num %) below the size limit of 10 μm. The mean values of grains finer than 4 μm for the A2 and A1 powders are <1 vol % (corresponding to values of 51 and 36 num %, respectively). The relatively high number of particles below the inhalable (10 μm) and respirable (4 μm) size limits (Brown et al., 2013) indicates that both powders are characterized by a fine GSD and attests to the potentially high number of alginate particles that could be inhaled if resuspended. Given the very high number of particles out of the total that can be easily resuspended and inhaled, it is suggested that the use of num % needs to be coupled with the commonly used vol % data to outline the magnitude of potentially inhalable powders.

The morphological variability of the grains forming both alginates is well represented by SMA plots of *Elng* (Fig. 2a) and *SLD* (Fig. 2b). In general, data resulting from the repeated analyses of the two alginates show a similar and consistent variability of trends for both *Elng* and *SLD* shape parameters. Namely, grains from both samples are characterized by a moderate *Elng*, with a maximum value (between 0.35 and 0.40) for particles in the range of 5 and 10 μm. For comparison, a reference *Elng* value for a fiber, as defined by the aspect ratio and morphology for respirable asbestos particles (Baron, 2014), is 0.667. This can safely allow ruling out the occurrence of a significant population of particles having a fibrous aspect ratio in the studied samples. Values of the two parameters for particles smaller than 2–3 μm should not be considered due to the resolution limit of the analytical method.

SLD markedly decreases from very high values (close to 1) for particles smaller than 10 μm, down to values of 0.75 for coarser sizes, suggesting an increase in the complexity of the external contour of coarse particle respect to those forming the fine fraction. This size-dependent variability in contour complexity is highly consistent with the significant presence of large, aggregated particles in the analyzed powders (Fig. S1, Supplementary Material). These are typically formed by clusters of very fine particles with sizes in the order of a few microns (Fig. S1) and are characterized by highly complex contours.

Phase composition

The identification of all the phases present in the commercial alginates investigated was carried out by combining the results of the SEM-EDS micromorphological and microchemical analyses and the XRPD investigation.

Microscopic examination of the dry samples reveals the obvious and abundant presence of diatomaceous earth (Fig. 3). The sample preparations show a high heterogeneity in size distribution, with numerous particles of 10–20 μm or larger. However, an aliquot of respirable particles (*i.e.*, those less than 4 μm in size) can be clearly seen at low magnification. Micrographs and morphological considerations suggest that these particles are derived from the fragmentation of original diatom shells, which are mostly found as aggregated clusters of various sizes (Fig. S2).

Closer examination of the micrographs reveals the presence of several particles that differ from diatomite particles in size, shape, and occasionally in backscattered electron yield. Some of these are

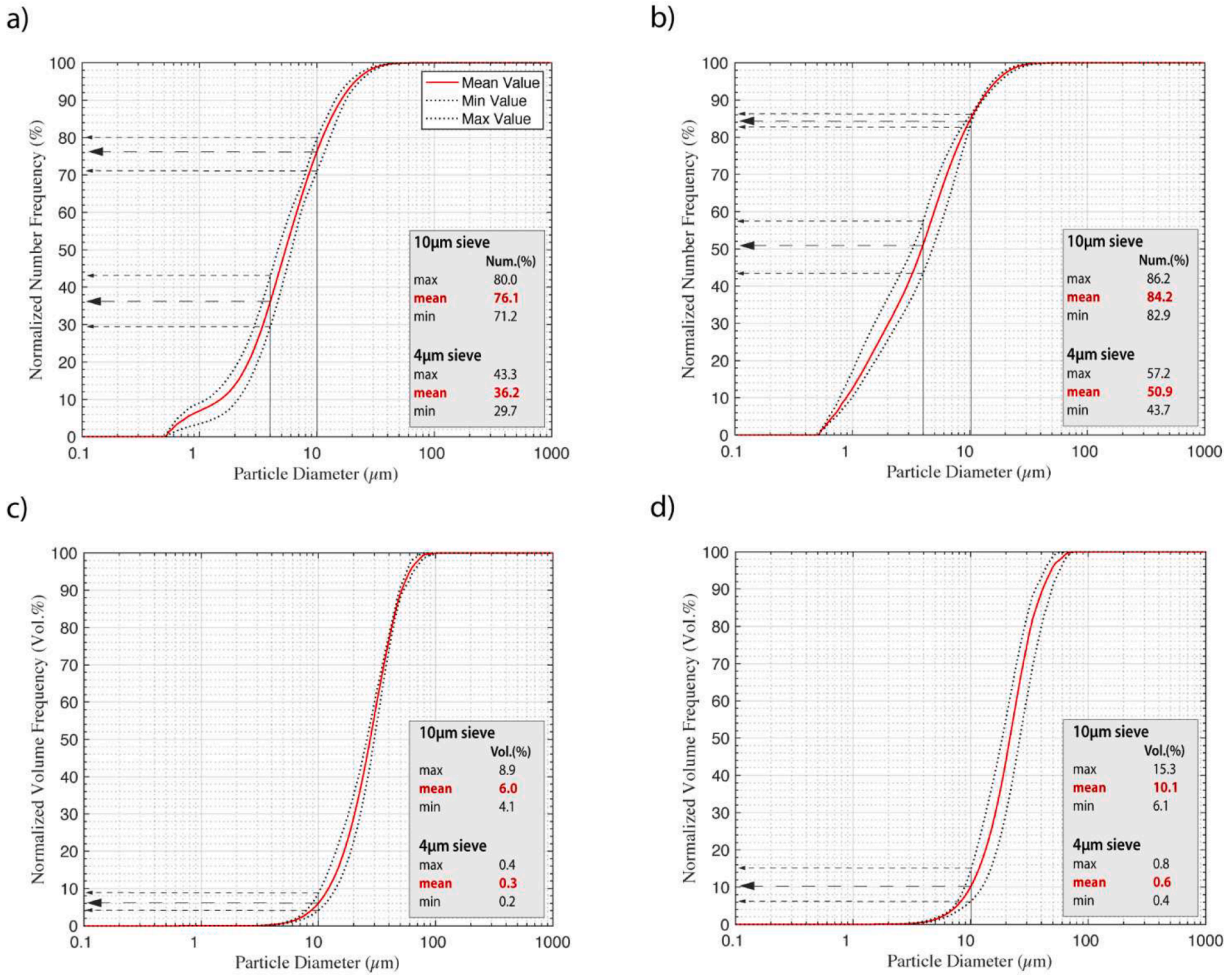

Fig. 1. Cumulative number and volume grain size distributions for sample A1 (a-c) and sample A2 (b-d). The mean cumulative GSD curve of the samples (red curve) is shown together with the maximum and minimum value of the uncertainty (dotted lines: absolute error). In the insets, the parameters for the numerical (a-b) and volumetric (c-d) distributions are also shown, together with the corresponding thoracic inhalable (10 μm) and respirable (4 μm) fractions of deposit.

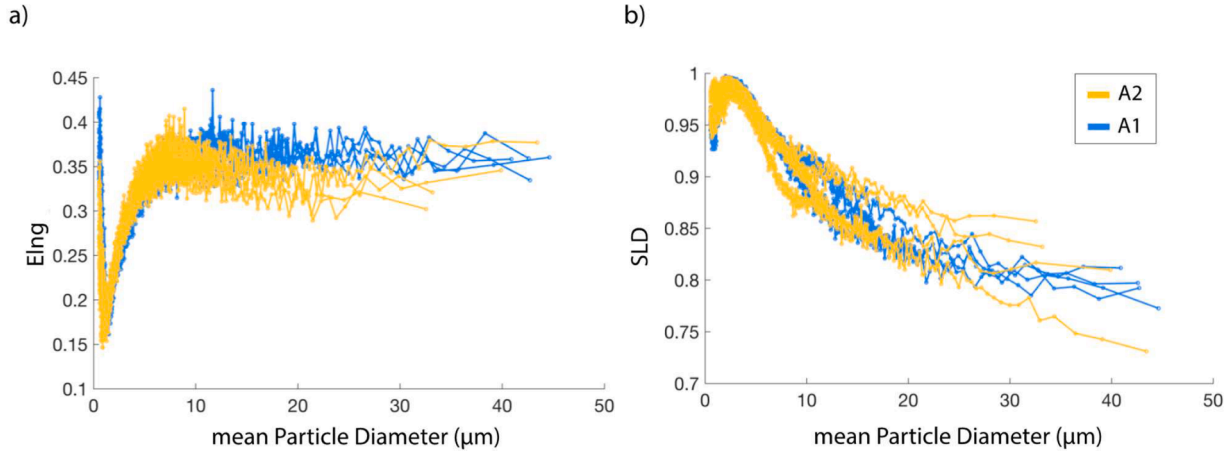

Fig. 2. Morphological variability of the grains from the two alginate samples (A1, A2). Moving average elongation, Elng, (a) and solidity, SLD, (b) are used to monitor the shape *versus* size variability of the grains.

highlighted by colored rectangles in the Fig. 3. Point X-ray microanalyses performed on such particles allowed their identification. The results are given in the Table 2. Both samples show the common presence of Ca sulfate, Na alginate and K fluortitanate, whereas particles attributed to periclase and talc were identified only in sample 1. This difference may be due to the limited representability of the electron microscopic investigations or, more likely, to the different formulations of the commercial products analyzed. All the phases detected, except talc, are materials commonly included in the formulation of dental alginates (Cook et al., 1986; Czeschowska et al., 2020).

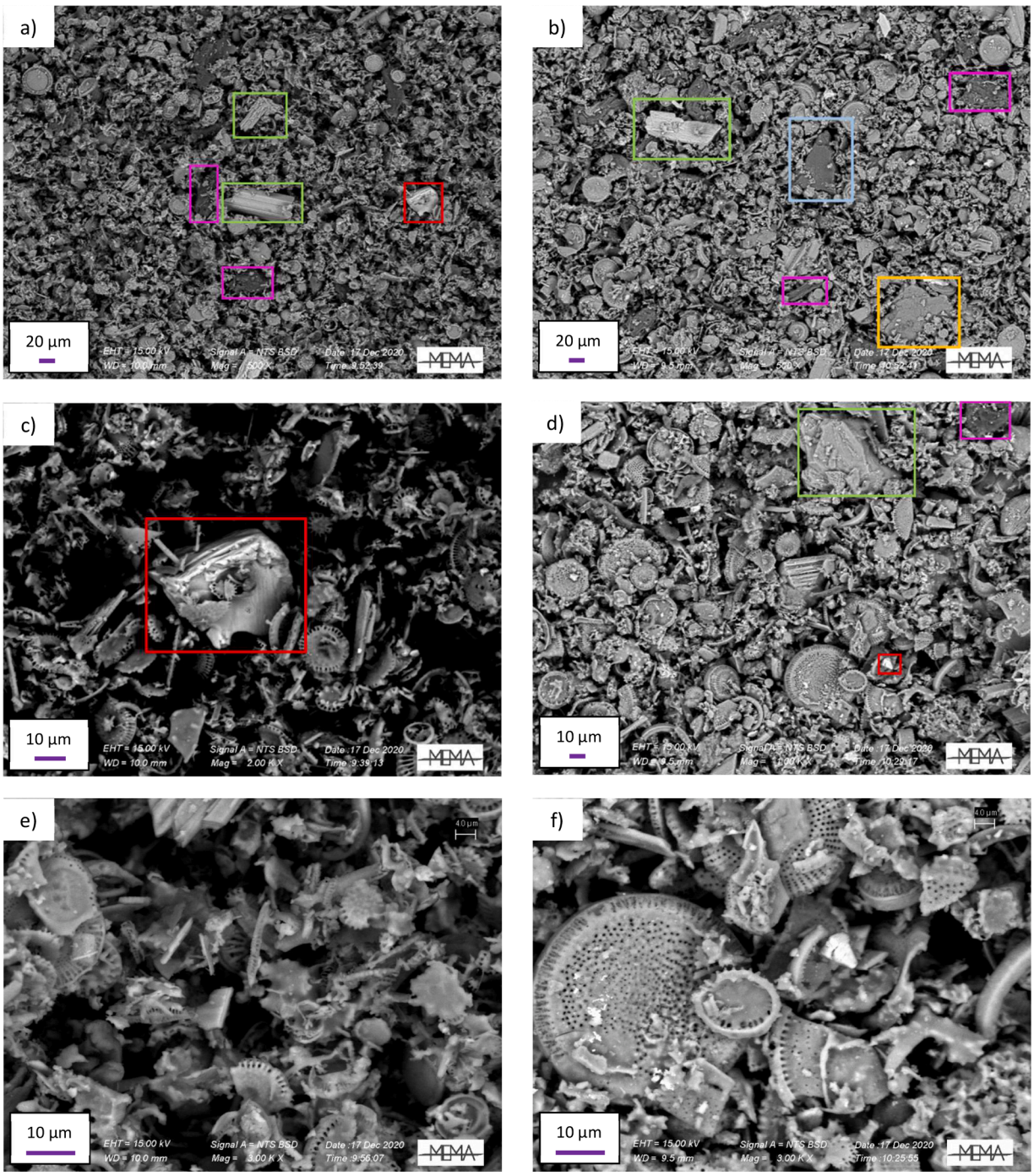

Fig. 3. Backscattered electron micrographs of the two samples investigated. a, c and e sample A1, b, d and f sample A2. Green, cyan, pink, yellow and red rectangles highlight particles of Ca sulfate, periclase, Na alginate, talc and K fluortitanate, respectively. Most of the unhighlighted particles consist of amorphous (or crystalline) silica (especially those with the typical diatomite shells). Magnification: 500X (a and b), 1000X (d), 2000X (c), 3000X (e and f).

The Rietveld refinement plot of the collected X-ray powder diffraction patterns is shown in Fig. 4.

Both samples are polyphasic and clearly show the presence of abundant cristobalite associated with gypsum, confirmed as the Ca source in the mixture. The results of the QPA are reported in Table 2. Among the phases detected, all those phases declared by the manufacturers were identified. A very good correlation between the XRPD and SEM results can be observed. In addition to cristobalite, gypsum, K fluortitanate and periclase (plus talc in sample A1, as declared in the material safety datasheet), other minor and associated phases were detected and quantified by QPA-XRPD (Table 2). They consist mainly of quartz, pseudowollastonite and wollastonite. The quartz is probably derived from the original mineralogical composition of the diatomite, where traces of this phase have been reported to occur frequently (Mohamedbakr and Burkitbaev, 2009; Zheng et al., 2018; Reka et al., 2021). In addition, a relevant amount of XRD amorphous phase (higher than 60 wt %) was quantified in both samples. The amorphous phase can be attributed to both diatomite particles, which partially retain their original state, and alginate-forming polymers.

Table 2
Phase composition of the samples investigated. *Values close to the detection limit; **Identified by morphology and microanalysis, attributable to both cristobalite and amorphous silica. N.d. – Not detected; N.i. – Not identified because amorphous and therefore not quantified in the subsequent Rietveld analysis.

Phase	sample A1		sample A2	
	XRD (wt%)	*SEM*	*XRD (wt%)*	*SEM*
Major phases				
Cristobalite	24.4(7)	✓**	28.4(9)	✓**
Gypsum	5.4(2)	✓	2.2(1)	✓
Minor phases				
Na alginate	*n.i.*	✓	*n.i.*	✓
K fluortitanate	0.1(1)*	✓	0.1(1)*	✓
Periclase	1.3(1)	✓	0.4(1)	*n.d.*
Pseudowollastonite	1.4(1)	*n.d.*	4.4(3)	*n.d.*
Wollastonite	0.8(1)	*n.d.*	2.5(1)	*n.d.*
Talc	2.6(2)	✓	*n.d.*	*n.d.*
Quartz	0.1(1)*	*n.d.*	0.2(1)	*n.d.*
Aragonite	*n.d.*	*n.d.*	0.6(1)	*n.d.*
Anatase	0.1(1)*	*n.d.*	*n.d.*	*n.d.*
amorphous (XRD)	63.8(9)	✓**	61.2(9)	✓**

Electron paramagnetic resonance (EPR)

The experimental room temperature EPR spectra of the two samples investigated are shown in Fig. 5. Both spectra are markedly similar and show two main spectral features: a signal (I) centered at ~165 mT, and a second (II), apparently asymmetric, whose most intense contribution occurs at ~330 mT. The spectra recorded at 80 K confirm the presence of both signals (Fig. 5). In addition, very weak multiple lines around 340 mT (III) allow the presence of a small amount of Mn(II).

The features of signals I and II (*i.e.*, their resonant fields at 165 mT and at 344 mT, corresponding to 4.2 and 2.0 g values) can both be associated with Fe(III) variably dispersed in the amorphous aliquot of both samples (Dunaeva et al., 2012). These spectral features, coupled with the small indentation visible at ~60 mT in the spectra of Fig. 5, can exhibit variable intensity ratios as a function of the total Fe(III) content in the amorphous phase and its distribution. Therefore, the presence of Fe(III) in other association contexts cannot be excluded, such as isolated ions in a crystalline matrix in rhombic distortion (Goodman and Raynor, 1970; Balan et al., 1999), or Fe(III) ions confined in superparamagnetic clusters/domains (Carbone et al., 2008). It is also worth noting that the occurrence of Fe(III) species with spectral features similar to those observed in the present study was previously reported by Di Benedetto et al. (2021). The observed spectral features were associated with a cristobalite-bearing material. It can be argued that, considering the asymmetry of the II signal, a small contribution to the overall intensity in this spectral region could be provided by some Cu(II) ions. On the other hand, considering the present context, the attribution of the dominant features to the Fe(III) species in an amorphous matrix seems the most likely.

Based on the experimental features, EPR spectroscopy does not reveal any paramagnetic species associated with cristobalite. In particular, Fe(III) probably belongs to additional phases in this composite material. Although very dilute in the samples investigated, the EPR spectra reveal the typical hyperfine structure of Mn, whose mean isotropic constant at about 10 mT allows attributing its presence to a paramagnetic, oxygen-based ligand crystal structure (Goodman and Raynor, 1970). Finally, it is worth mentioning that, as shown in the inset of Fig. 5a, no evidence of EPR signals attributable to radical species was detected, within the experimental sensitivity.

Transmission electron microscopy

TEM investigations were focused on the finest fraction of the samples in order to couple information on the aerodynamic properties of the investigated materials with that on the structural arrangement of the particles. For both samples, the majority of the grains are composed of crystalline silica, as proved by chemical analyses and electron diffraction images obtained from each grain. The crystallinity is shown by the selected area electron diffraction (SAED) patterns (Fig. 6). The size of the grains never exceeds 2 μm and most have a geometric diameter of 0.5 μm. Often grains appear aggregated and enveloped in thin sheets as shown in Fig. 6a where SAED (top left) is related to enveloping sheet silicate (Fig. 6a), more or less irregular and perforated (Fig. 6b).

The size of these aggregates is less than 4 μm, and therefore the constituent grains are of a size considered respirable for humans. In fact, by applying the relation $d^2_{aero}/d^2_{geo} = \rho_{part}/\rho_{aero}$ where $\rho_{aero} = 1\ g/cm^3$ (Barthel et al., 1999) and assuming for crystalline silica a ρ_{part} value of about $2.2\ g/cm^3$, the most grains have $d_{aero} < 1.6\ \mu m$ and hence a high possibility to penetrate deeply into regions of the respiratory tract (*e.g.*, Brown et al., 2013).

Discussion and conclusions

Respirable fraction of the impression materials

Data reported in Fig. 1 show a very fine grain-size distribution for the two alginates. Despite the low vol % of powders below the "thoracic" inhalable size (10 μm), they represent more than 70 num % of the samples, indicating that a very high number of particles can be easily resuspended from a given aliquot of alginate powder. This, in turn, suggests a potentially high risk to human health due to the inhalation hazard of this abundant fraction of the deposit. On the other hand, the datasheets provided for the studied alginates report a composition of the powder largely dominated by the presence of siliceous diatomites, with an average content of 65–80 wt % and 50–75 wt % for samples A2 and A1, respectively. Furthermore, the average grain size of natural diatomites is typically very fine, with about 4.6–25.4 wt % of the deposits below 4 μm, and 11.4–71.5 wt % below 10 μm (Nattrass et al., 2015). These data agree well with those obtained here from SEM and TEM imaging (Figs. 3 and 6), where the presence of a finer fraction of the deposit is largely dominated by numerous fragmented diatomaceous shells, present both as individual particles and as aggregated clusters (Fig. 3 and Fig. S2). These data, together with the GSD results, shed new light on the real risk to human health associated with the manipulation of these alginates by clearly demonstrating the abundant presence of siliceous particles in the respirable and breathable fraction of the powders. This fine, silica-enriched fraction of the deposit is also the most suitable for remobilization and subsequent inhalation, due to the very low mass and terminal velocity of the diatomaceous particles. For example, recent experiments on the resuspension of volcanic ash clearly show that the maximum yield of ash during wind-induced resuspension events is below 10 μm (Etyemezian et al., 2019).

The presence of particle aggregates (Fig. S2) in the powders analyzed, as evidenced by the occurrence of progressively lower SLD values (Fig. 2), and thus an increased perimeter complexity for coarse grains, possibly masks the true amount of fine powder and could effectively reduce the hazard associated with the manipulation of these alginates. In fact, the segregation of a finer powder fraction in favor of the formation of large particle clusters acts as a selective subtraction of the very fine grains from the whole deposit. The occurrence of the latter process is clearly highlighted in Fig. S2 (Supplementary Material), where the amount of respirable fraction in each sample scales with the average value of SLD for the particles coarser than 30 μm. However, since the efficiency of the particle aggregation process has been shown to be strongly related to environmental conditions (*i.e.*, collision kinetic energy and relative humidity; *e.g.*, Telling et al., 2013), and considering the normal preparation procedures of these alginates, we suggest that the measured amount of fine particles in the two powders possibly represents a minimum value with respect to the actual content of these particles, which are also largely present in the observed aggregates.

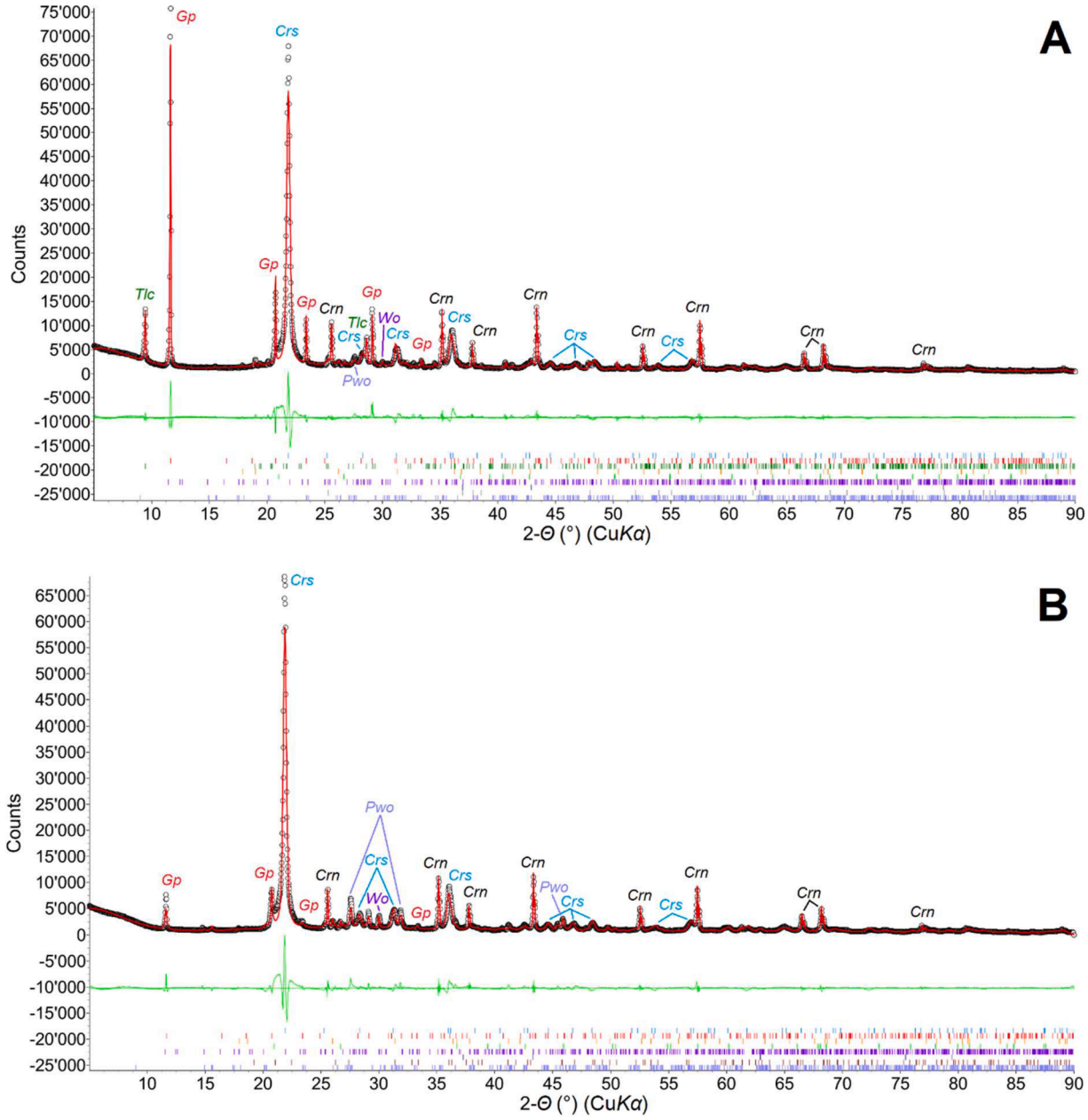

Fig. 4. Rietveld refinement plots of the XRPD patterns collected at RT for the samples investigated (A and B represent Rietveld plots for samples A1 and A2, respectively). The experimental profile is represented by black dots, the continuous red line is the calculated pattern, while the lower green curve is the difference between calculated and observed intensities. Vertical ticks mark the position of the reflections for the identified phases. Peaks belonging to the major constituents are also highlighted along with that of corundum (used as an internal standard). Namely, Crn, Crs, Gp, Pwo, Tlc, and Wo stand for corundum, cristobalite, gypsum, pseudowollastonite, talc, and wollastonite, respectively (Warr, 2021).

Occurrence of cristobalite and wollastonite in the impression materials

From a toxicological point of view, the most prominent phases identified are cristobalite and wollastonite/pseudowollastonite polytypes (Table 2). The amount of cristobalite is higher than 24 wt % in both samples and, regardless of whether the quantified amorphous content is attributed to the residual part of the amorphous silica of the diatomite, it would represent a fraction of at least 1/3 of the total silica contained in each sample. Accordingly, the alginate samples investigated in this study can be classified, on the basis of their cristobalite content, among other cristobalite-rich materials processed in occupational settings (*e.g.*, artificial stone, >70 wt % crs, Di Benedetto et al., 2019; and gold microcasting, ~25 wt % crs, Phetrattanarangsi et al., 2017). Adverse health effects on workers have been reported in all of the settings considered.

The detection of cristobalite in calcium alginate mixtures was first reported by Barbieri et al. (2020). These authors confirmed (by XRPD) the presence of cristobalite both in a commercial sample and in the lungs of volunteers in a study designed to assess the relationship with exposure to respirable dusts of alginate impression materials. It was shown quantitatively that cristobalite fragments with a structural coherence of about 30 nm may be common in the respirable fraction.

The experimental presence of a relevant amount of cristobalite in the samples studied must be related to the use of diatomite in the formulation of the mixture. In fact, this material is often subjected to thermal calcination treatments aimed at purifying the silica content from other components, such as organic matter and carbonates. These and other phases (usually clay minerals) are closely related to the sedimentation of

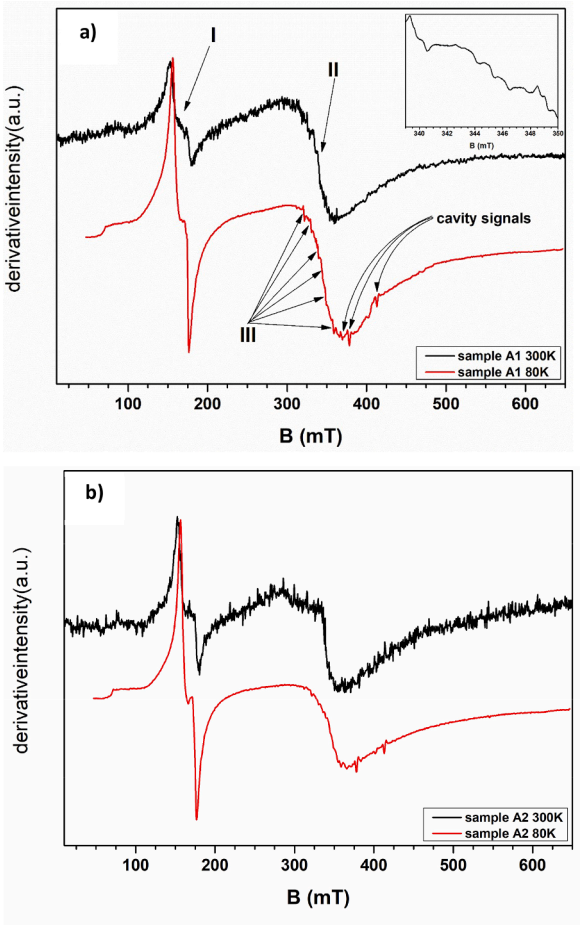

Fig. 5. Experimental EPR spectra recorded at room temperature (in black) and at 80 K (in red) for the investigated samples A1 (a) and A2 (b). In the inset (a), detail of the spectrum for sample A1 at 80 K in the region around $g = 2$.

diatomaceous earths (Cleveland 1958; Zheng et al., 2018). The use of thermal treatment in the studied samples is evidenced by the occurrence of high-temperature phases such as aragonite, wollastonite, and pseudowollastonite. The thermal treatments used are usually carried out at temperatures between 900 and 1200 °C, with the possible addition of some mineral fluxes (Zheng et al., 2018). In the case of the investigated samples, one manufacturer declares the use of calcined diatomite with the addition of Na_2CO_3 flux. The thermal treatment is not carried out on the diatomite after its incorporation into the alginate formulation. Treatment at such high temperatures would result in severe damage or destruction of the alginate fraction. Accordingly, the presence of cristobalite in the diatomite fraction is foreseen before the mixing step, which means that the raw calcined diatomite powders already contain a relevant amount of cristobalite. In fact, the production of calcium alginate mixtures can be classified as closely related to diatomite production in terms of risk assessment.

The presence of wollastonite/pseudowollastonite species is due to the same thermal treatment. In fact, these polytypes (especially pseudowollastonite, which is usually synthesized at temperatures higher than 1400 °C) can be obtained by the reaction of amorphous silica and calcium carbonate at high temperatures (Morey, 1964; De Aza et al., 1999; De Aza et al., 2000), according to the following reaction:

$$SiO_2 + CaCO_3 \rightarrow CaSiO_3 + CO_2 \quad (1)$$

In the original sedimentary mineral assemblage, the presence of calcite has been previously documented (Zheng et al., 2018). Accordingly, some or all of the calcium content associated with calcite may have been converted to a calcium silicate polytype.

Overall, our results suggest the following general scheme (Fig. 7) for the introduction of crystalline silica into the production cycle of alginate impression materials.

Concluding remarks on the risk associated with the preparation and use of alginate

A very relevant point concerning the samples of alginate mixtures studied is the absence of radical species. Since the diatomite was subjected to a thermal treatment at a temperature higher than 450 °C, radical species in the diatomite, if present, are probably annihilated by recombination processes (Fubini et al., 1990; Ikeya, 1993). The absence of radicals is even more relevant when the investigated materials are compared with other raw materials containing cristobalite, *e.g.*, the filler for artificial stone (Di Benedetto et al., 2021). In the case of the dust used as filler for artificial stone, the presence of long-lived superoxide radicals has been considered as a cofactor to define the inflammatory effects. However, the absence of radical species in the alginates studied, coupled with the fact that these materials are associated with clinical evidence of pathological effects, suggests that other factors could play a decisive role in the toxicological effects of these phases.

Recently, Pavan et al. (2020) demonstrated that Nearly Free Silanols (NFS), surface chemical hydroxyl terminations of α-quartz, play a central role in explaining the toxicological behavior of such mineral species. Subsequent investigations by the same authors suggest that the same role is played by other polymorphs of the silica group of minerals, such

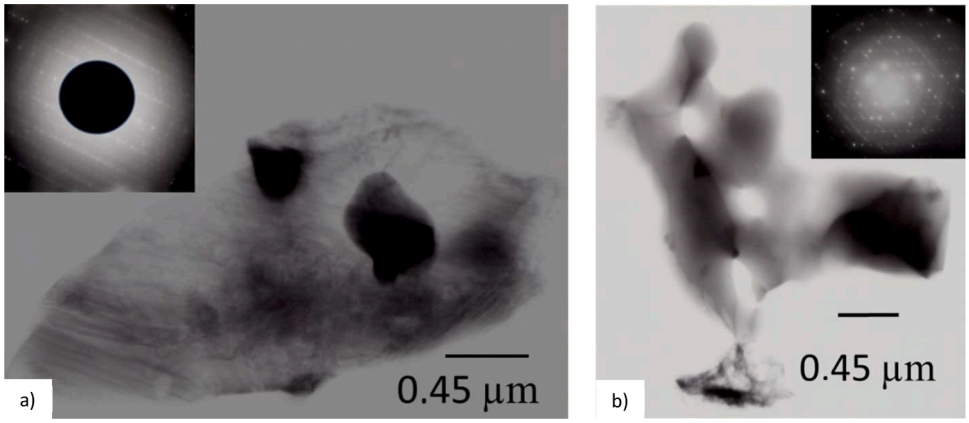

Fig. 6. Representative TEM images of aggregates of crystalline silica grains from samples A1 (a) and A2 (b). SAED patterns highlighting the crystalline nature of the grains are shown in the insets. The top left and the top right SAEDs are related to enveloping sheet silicate and to silica grains, respectively. The central black disk in the inset of image "a" is the pinhole used to partially obscure the sample surface from the high-brightness transmission beam.

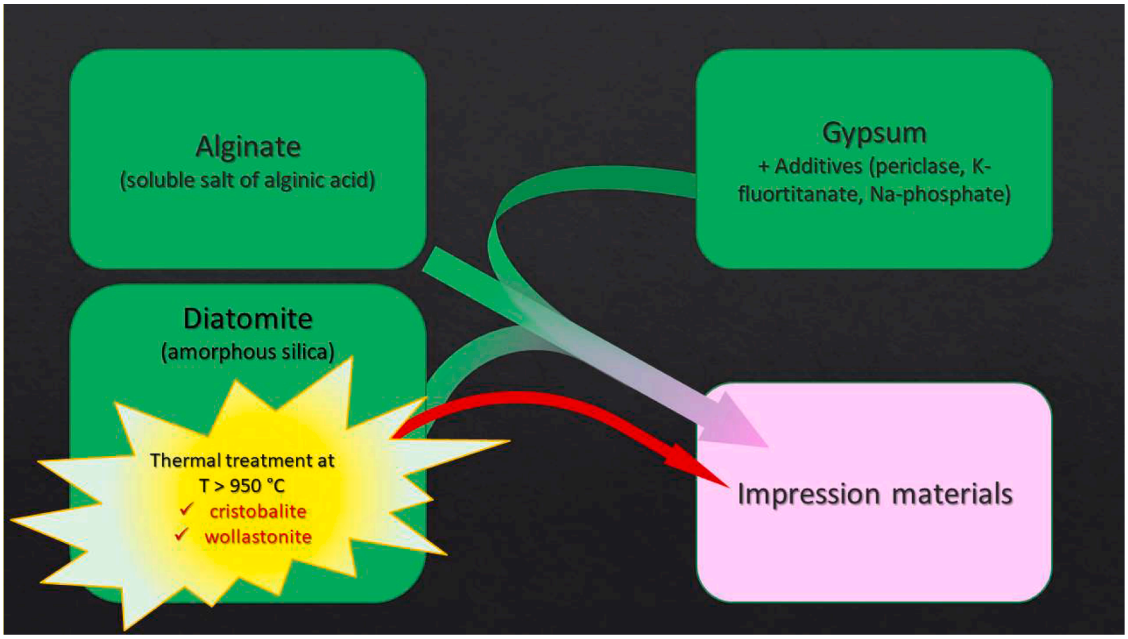

Fig. 7. Schematic representation of the preparation of impression alginate materials: alginate salts are mixed with diatomite and gypsum. In diatomite, amorphous silica has been partially converted to cristobalite by high temperature treatment. In the same process, wollastonite is obtained by reaction of silica and calcium carbonate.

as cristobalite (Pavan et al., 2022). The concentration of NFS tends to increase in samples with high specific surfaces and especially in freshly fractured surfaces. We propose that the NFS factor also plays a relevant role for cristobalite-bearing flours/dust. In fact, cristobalite domains in the diatomite structure can be considered as a high specific surface area silica system.

Similar to silica polymorphs, the potential health effects of exposure to wollastonite particles and fibers are of primary concern (Maxim and McConnell, 2005). Studies of wollastonite toxicity have been conducted despite the lack of specific regulation because this particulate contaminant is typically included in respirable dusts as a whole. OSHA established a permissible exposure limit (PEL) for calcium silicate of 15 mg/m^3. NIOSH recommended a PEL of 5 mg/m^3 for wollastonite in respirable dusts, and ACGIH proposed a TLV of 10 mg/m^3 for calcium silicate in dusts (Maxim and McConnell, 2005). A review of all the toxicological aspects of wollastonite presented in the same study did not provide convincing evidence to support a risk assessment at this time. However, these authors concluded that, in the absence of sufficiently developed epidemiological cohorts, monitoring of occupational exposures and studies of the tissue reactivity of wollastonite are recommended. In this context, the co-occurrence of wollastonite (a suspected toxicant) and cristobalite (a carcinogen) is an additional warning for preventive purposes. Interestingly, the morphometric study, which gives the elongation parameter, shows that the elongation of the particles almost never approaches the ratio characteristic of a fibrous habitus, indicating that the presence of fibers in the samples studied is almost negligible.

In conclusion, this study has shown a way to identify the presence of hazardous particles that can be released by airborne dispersion during the preparation and manipulation of calcium alginate mixtures for impression materials. In particular, the presence of a significant amount of cristobalite is confirmed in particles whose size can easily fall within the limits for respirable dusts, in full agreement with the results of Barbieri et al. (2020). In terms of prevention, it should be noted that the thermal treatment that modifies the composition of the initial phase of diatomite, crystallizing both cristobalite and calcium silicate polytypes, is carried out in a step prior to mixing with other raw materials. In fact, it can be concluded that the most critical step for worker exposure occurs during the preparation of the mixture. This conclusion is also in line with the results of Barbieri et al. (2020). Conversely, the use of these impression materials in the dental laboratories, where calcium alginates are mixed with water and allowed to set, is likely to be the source of a small amount of respirable particles. The risk associated with exposure to calcium alginate dusts could therefore be considered to be due to the commercial distribution of diatomite materials and therefore falls fully within the risk already established for such materials. The presence of cristobalite in calcium alginates can be empirically related to the severity of the health effects, as in other industrial production (diatomite production, artificial stone, gold microcasting). The significant content of crystalline cristobalite, as well as that of calcium silicates, associated with a high fraction of respirable dust (> 30 % of the total number of particles), requires a redefinition of dental alginates based on their health risks, taking into account, in particular, the effective production cycles as well as the times and places of potential exposure. Likewise, we recommend the adoption of prevention strategies to be applied in the production of alginates, very close to those adopted in the primary production of diatomite.

Declaration of Competing Interest

The authors declare that they have no known competing financial interests or personal relationships that could have appeared to influence the work reported in this paper.

Acknowledgements

The Interdepartmental Centres for Crystallography (CRIST) and for Microscopy and Microanalysis (MEMA) of the University of Florence (Italy) are gratefully acknowledged for provision of experimental time and access to the facilities. Laura Chelazzi and Samuele Ciattini (CRIST) are acknowledged for their help in the preliminary XRPD and XRF characterization of the materials, as well as Laura Chiarantini for her help during the SEM-EDS investigations. Sandra Ristori, of the Department of Chemistry (University of Florence) is warmly acknowledged for granting access to the EPR lab.

FDB acknowledges the University of Ferrara for funding this research

under the FAR2021 and FAR2022 programs, as well as the University of Florence for funding under the Progetto di Ateneo 2021 program.

Supplementary materials

Supplementary material associated with this article can be found, in the online version, at doi:10.1016/j.heha.2023.100083.

References

Balan, E., Allard, T., Boizot, B., Morin, G., Muller, J.P., 1999. Structural Fe^{3+} in natural kaolinites: new insights from electron paramagnetic resonance spectra fitting at X and Q-band frequencies. Clays Clay Miner. 47, 605–616.

Barbieri, P.G., Somigliana, A., Carradori, G., 2020. Silicosi severa da terre di diatomee nella produzione di alginato ad uso odontoiatrico: uno studio necroscopico. Med. Lav. 111 (3), 222–231 (in Italian).

Barthel, H., Heinemann, M., Stintz, M., Wessely, B., 1999. Particle sizes of fumed silica. Chem. Eng. Technol. 21 (9), 745–752.

Baron (2014) https://www.cdc.gov/niosh/docs/2014-151/pdfs/chapters/chapter-fi.pdf (Accessed on October 22, 2022).

Brown, J.S., Gordon, T., Price, O., Asgharian, B., 2013. Thoracic and respirable particle definitions for human health risk assessment. Part. Fibre Toxicol. 10, 1–12.

Carbone, C., Di Benedetto, F., Sangregorio, C., Marescotti, P., Pardi, L.A., Sorace, L., 2008. Multifrequency EMR and Magnetic Characterization of Synthetic Powdered Hematite. J. Phys. Chem. C 112 (27), 9988–9995.

Checkoway, H., Heyer, N.J., Demers, P.A., Breslow, N.E., 1993. Mortality among workers in the diatomaceous earth industry. Br. J. Ind. Med. 50 (7), 586–597.

Cleveland, George Barrie, 1958. Poverty Hills diatomaceous earth deposit, Inyo County, California. California J. Mines Geol. 54 (3), 305–316.

Cook, W., 1986. Alginate dental impression materials: chemistry, structure and properties. J. Biomed. Mater. Res. 20, 1–24.

Czechowska, J., Zima, A., Ślósarczyk, 2020. Comparative study on physicochemical properties of alpha-TCP /calcium sulphate dihydrate biomicroconcretes containing chitosan, sodium alginate or methylcellulose. Acta Bioeng. Biomech. 22 (1), 47–56.

De Aza, P.N., Luklinska, Z.B., Anseau, M.R., Guitian, F., De Aza, S., 1999. Bioactivity of pseudowollastonite in human saliva. J. Dent. 27 (2), 107–113.

De Aza, P.N., Luklinska, Z.B., Martinez, A., Anseau, M.R., Guitian, F., De Aza, S., 2000. Morphological and structural study of pseudowollastonite implants in bone. J. Microsc. 197 (1), 60–67.

Di Benedetto, F., Giaccherini, A., Montegrossi, G., Pardi, L.A., Zoleo, A., Capolupo, F., Innocenti, M., Lepore, G.O., d'Acapito, F., Capacci, F., Poli, C., Iaia, T.E., Buccianti, A., Romanelli, M., 2019. Chemical variability of artificial stone powders in relation to their health effects. Sci. Rep. 9, 6531. https://doi.org/10.1038/s41598-019-42238-2.

Di Benedetto, F., Giaccherini, A., Romanelli, M., Montegrossi, G., Belluso, E., Capella, S., Zoleo, A., Arcangeli, G., Marinaccio, A., Gottardo, O., Capacci, F., 2021. A study of radicals in industrial raw cristobalite powders. Phys. Chem. Miner. 48, 9.

Dunaeva, E.S., Uspenskaya, I.A., Pokholok, K.V., Minin, V.V., Efimov, N.N., Ugolkova, E. A., Brunet, E., 2012. Coordination and RedOx ratio of iron in sodium-silicate glasses. J. Non Cryst. Solids 358 (23), 3089–3095.

Etyemezian, V., Gillies, J.A., Mastin, L.G., Crawford, A., Hasson, R., Van Eaton, A.R., Nikolich, G., 2019. Laboratory experiments of volcanic ash resuspension by wind. J. Geophys. Res.: Atmos. 124, 9534–9560. https://doi.org/10.1029/2018JD030076.

Fubini, B., Giamello, E., Volante, M., Bolis, V., 1990. Chemical functionalities at the silica surface determining its reactivity when inhaled. Formation and reactivity of surface radicals. Toxicol. Ind. Health 6 (6), 571–598.

Goodman, B.A., Raynor, J.B., 1970. Electron Spin resonance of transition metal complexes. Adv. Inorg. Chem. Radiochem. 13, 135–362.

Gualtieri, A.F., Riva, V., Bresciani, A., Maretti, S., Tamburini, M., Viani, A., 2014. Accuracy in quantitative phase analysis of mixtures with large amorphous contents. The case of stoneware ceramics and bricks. J. Appl. Crystallogr. 47, 835–846.

Hattab, F.N., 2019. Local and systemic effects of fluoride in alginate impression materials: a review. Int. J. Exp. Dental Sci. 8 (2), 51–57.

Ikeya, M., 1993. New Applications of Electron Paramagnetic Resonance: ESR Dating, Dosimetry, and Spectroscopy. World Scientific, Singapore.

International Agency for Research on Cancer, IARC Monographs: arsenic, Metals, Fibres, and Dusts, 100C (2012).

Leibrandt, S., Le Pennec, J.L., 2015. Towards fast and routine analyses of volcanic ash morphometry for eruption surveillance applications. J. Volcanol. Geotherm. Res. 297, 11–27.

Maxim, L.D., McConnell, E.E., 2005. A review of the toxicology and epidemiology of wollastonite. Inhal. Toxicol. 17 (9), 451–466.

Mohamedbakr, H., Burkitbaev, M., 2009. Elaboration and characterization of natural diatomite in Aktyubinsk/Kazakhstan. Open Mineral. J. 3, 12–16.

Morey, G.W., 1964. Phase-equilibrium Relations of the Common Rock-Forming Oxides Except Water, 440. US Government Printing Office.

Nattrass, C., Horwell, C.J., Damby, D.E., Kermanizadeh, A., Brown, D.M., Stone, V., 2015. The global variability of diatomaceous earth toxicity: a physicochemical and *in vitro* investigation. J. Occup. Med. Toxicol. 10 (23), 1–16. https://doi.org/10.1186/s12995-015-0064-7.

Pavan, C., Bellomo, C., Cananà, S., Tomatis, M., Casado, G.E., Mino, L., Lison, D., Turci, F., 2022. Nearly free silanols on silica surface: a new paradigm for particle toxicity. In: Abstract in: Proceedings of the XXII IMA meeting. Lyon, p. 458, 18-22 July 2022.

Pavan, C., Santalucia, R., Leinardi, R., Fabbiani, M., Yakoub, Y., Uwambayinema, F., Ugliengo, P., Tomatis, M., Martra, G., Turci, F., Lison, D., Fubini, B., 2020. Nearly free surface silanols are the critical molecular moieties that initiate the toxicity of silica particles. Proc. Natl Acad. Sci. 117 (45), 1–11.

Phetrattanarangsi, T., Puncreobutr, C., Khamkongkaeo, A., Thongchai, C., Sakkomolsri, B., Kuimalee, S., Kidkhunthod, P., Chanlek, N., Lohwongwatana, B., 2017. The behavior of gypsum-bonded investment in the gold jewelry casting process. Thermochim. Acta 657, 144–150. https://doi.org/10.1016/j.tca.2017.09.008.

Picciotto, S.;., Neophytou, A.M., Brown, D.M., Checkoway, H., Eisen, E.A., Costello, S., 2018. Occupational silica exposure and mortality from lung cancer and nonmalignant respiratory disease: G-estimation of structural nested accelerated failure time models. Environ. Epidemiol. 2 (3), e029. https://doi.org/10.1097/EE9.0000000000000029.

Porrelli, D., Berton, F., Camurri Piloni, A., Kobau, I., Stacchi, C., Di Lenarda, R., Rizzo, R., 2020. Evaluating the stability of extended-pour alginate impression materials by using an optical scanning and digital method. J. Prosthet. Dent. 125, 189, 2021e1-e7.

Reka, A.A., Pavlovski, B., Fazlija, E., Berisha, A., Pacarizi, M., Daghmehchi, M., Sacalis, C., Jovanovski, G., Makreski, P., Oral, A., 2021. Diatomaceous Earth: characterization, thermal modification, and application. Open Chem. 19, 451–461.

Snyder, R.L., Bish, D.L., 1989. Quantitative analysis. In: Snyder, R.L., Bish, D.L. (Eds.), Modern Powder Diffraction. De Gruyter, Berlin, pp. 101–144.

Telling, J., Dufek, J., Shaikh, A., 2013. Ash aggregation in explosive volcanic eruptions. Geophys. Res. Lett. 40 (10), 2355–2360.

Warr, L.N., 2021. IMA–CNMNC approved mineral symbols. Mineral. Mag. 85 (3), 291–320.

Yamamoto, K., Yuguchi, Y., Torger Stokke, B., Sikorski, P., Bassett, D.C., 2019. Local structure of Ca^{2+} alginate hydrogels gelled via competitive ligand exchange and measured by small angle X-Ray scattering. Gels 5 (3), 1–13.

Zheng, R., Ren, Z., Gao, H., Zhang, A., Bian, Z., 2018. Effects of calcination on silica phase transition in diatomite. J. Alloys Compd. 757, 364–371.